Quantifying metal artefact reduction using virtual monochromatic dual-layer detector spectral CT imaging in unilateral and bilateral total hip prostheses

R.H.H. Wellenberg [a,*], M.F. Boomsma [b], J.A.C. van Osch [b], A. Vlassenbroek [c], J. Milles [d], M.A. Edens [e], G.J. Streekstra [a], C.H. Slump [f], M. Maas [a]

[a] Department of Radiology, Academic Medical Centre, Amsterdam, The Netherlands
[b] Department of Radiology, Isala, Zwolle, The Netherlands
[c] Philips Medical Systems, Brussels, Belgium
[d] Philips Medical Systems, Eindhoven, The Netherlands
[e] Department of Innovation and Science, Isala, Zwolle, The Netherlands
[f] MIRA Institute for Biomedical Technology and Technical Medicine, University of Twente, Enschede, The Netherlands

ARTICLE INFO

ABSTRACT

Purpose: To quantify the impact of prosthesis material and design on the reduction of metal artefacts in total hip arthroplasties using virtual monochromatic dual-layer detector Spectral CT imaging.
Methods: The water-filled total hip arthroplasty phantom was scanned on a novel 128-slice Philips IQon dual-layer detector Spectral CT scanner at 120-kVp and 140-kVp at a standard computed tomography dose index of 20.0 mGy. Several unilateral and bilateral hip prostheses consisting of different metal alloys were inserted and combined which were surrounded by 18 hydroxyapatite calcium carbonate pellets representing bone. Images were reconstructed with iterative reconstruction and analysed at monochromatic energies ranging from 40 to 200 keV. CT numbers in Hounsfield Units (HU), noise measured as the standard deviation in HU, signal-to-noise-ratios (SNRs) and contrast-to-noise-ratios (CNRs) were analysed within fixed regions-of-interests placed in and around the pellets.
Results: In 70 and 74 keV virtual monochromatic images the CT numbers of the pellets were similar to 120-kVp and 140-kVp polychromatic results, therefore serving as reference. A separation into three categories of metal artefacts was made (no, mild/moderate and severe) where pellets were categorized based on HU deviations. At high keV values overall image contrast was reduced. For mild/moderate artefacts, the highest average CNRs were attained with virtual monochromatic 130 keV images, acquired at 140-kVp. Severe metal artefacts were not reduced. In 130 keV images, only mild/moderate metal artefacts were significantly reduced compared to 70 and 74 keV images. Deviations in CT numbers, noise, SNRs and CNRs due to metal artefacts were decreased with respectively 64%, 57%, 62% and 63% (p < 0.001) compared to unaffected pellets. Optimal keVs, based on CNRs, for different unilateral and bilateral metal hip prostheses consisting of different metal alloys varied from 74 to 150 keV. The Titanium alloy resulted in less severe artefacts and were reduced more effectively compared to the Cobalt alloy.
Conclusions: Virtual monochromatic dual-layer Spectral CT imaging results in a significant reduction of streak artefacts produced by beam-hardening in mild and moderate artefacts by improving CT number accuracy, SNRs and CNRs, while decreasing noise values in a total hip arthroplasty phantom. An optimal monochromatic energy of 130 keV was found ranging from 74 keV to 150 keV for different unilateral and bilateral hip prostheses consisting of different metal alloys.

1. Introduction

Metallic implants are known to generate artefacts in computed tomography (CT) images due to beam-hardening, scatter effects and photon-starvation [1]. These artefacts impede the diagnostic accuracy of soft tissue and bone pathology in patients after total hip arthroplasty. The beam-hardening effect is caused by the absorption of the polychromatic X-ray beam [2]. Since low-energy X-ray photons are attenuated more easily than the remaining high-energy photons, polychromatic beam transmission does not follow the exponential decay seen with a monochromatic X-ray. This process particularly generates artefacts when high atomic number materials such as metals are present [1]. The severity of these metal artefacts generally increases with the atomic numbers of the implant material.

Metal artefacts can be reduced using virtual monochromatic images computed from Dual-Energy CT or Spectral CT scans by eliminating the beam-hardening effect [3–8]. Monochromatic images reported in kiloelectron volt (keV), depict objects as if the X-ray source produced X-ray photons at a single energy level only, instead of a range of X-ray photons up to a certain maximum energy or peak kilovoltage (kVp) in conventional CT [7]. These monochromatic images can be computed from the CT reconstructions from projection data with low and high average photon energy. Extrapolating to high energies results in monochromatic images with reduced metal artefacts compared to those at low energies due to reduced beam-hardening effects.

Several Dual-Energy CT studies investigated the value of virtual monochromatic imaging in the reduction of metal artefacts with optimal energies varying between 95 and 190 keV [5,6,9–16]. In these studies, the benefits of high keV virtual monochromatic imaging regarding metal artefacts is well recognized for several Dual-Energy CT implementations. However, a thorough quantitative evaluation of the effect of the type of material used for the implant on the performance of virtual monochromatic imaging as a tool for metal artefact reduction has not been investigated yet. Also, the quantification of metal artefact reduction using a novel dual-layer detector approach has not previously been described.

Hence, the aim of this study was to quantify metal artefact reduction in the CT imaging of different unilateral and bilateral hip prostheses types using dual-layer detector Spectral CT imaging at various monochromatic energies. For the evaluation of the residual metal artefacts we use quantitative CT image quality parameters i.e. CT number accuracy, noise values, signal-to-noise-ratios (SNRs) and contrast-to-noise-ratios (CNRs).

2. Materials and methods

2.1. Spectral CT imaging using dual-layer detector technique

The recently introduced dual-layer detector technique detects two different photon x-ray spectra simultaneously enabling a spectral separation in the projection space without the need of spatial and temporal interpolations [17]. This system consists of a single tube and uses detectors with simultaneous high and low energy discrimination where the low energy photons are captured in the first layer and the high energy photons are captured in the second layer of the detector. With this approach virtual monochromatic images can be extracted and extrapolated ranging from 40 up to 200 keV.

2.2. Hip phantom and prostheses

The custom made hip phantom consists of polymethyl methacrylate (PMMA) or Perspex with dimensions of 320 mm width, 130 mm height, and 290 mm depth (Fig. 1). Additional PMMA shields were placed below and on top of the phantom to increase the sagittal diameter to 190 mm, based on the water-equivalent diameter of 291.5 mm and coronal diameter of 320 mm derived from a body mass index of 25 using a formula of Menke et al. (Fig. 1) [18]. The phantom was filled with water and different prosthetic configurations were inserted. Since we wanted to determine the effect of different prosthetic composites and the use of unilateral and bilateral prostheses we have composed six prosthetic compositions referred to as 'Boxes', shown in Table 1. Scans were obtained with and without the insertion of three different hip prostheses with different stem, head and cup composites. The prostheses were fixated with custom-made PMMA moulds in order to prevent movement and provide correct alignment at the middle of the phantom. The phantom contained 18 cylindrical hydroxyapatite calcium carbonate pellets representing bone with a certified density calibration and documented tolerance of ±0.5% [19] placed at relevant radiological zones in the femur (the Gruen zones, pellets 1–7) and acetabulum (DeLee and Charnley zones, pellets 0 and 8) [20,21]. On each side 9 pellets with a height and diameter of 10 mm were fixated onto PMMA pillars to ensure correct alignment of the pellets at the middle of the phantom (Fig. 1).

2.3. Image acquisition and reconstruction

Scans were reconstructed with iterative reconstruction and were analysed with a standardized measurement template mask. The phantom was scanned on a Philips IQon 128-slice dual-layer detector Spectral CT scanner at standard dose with a Computed Tomography Dose Index (CTDI) of 20.0 mGy at 120-kVp and 140-kVp. Static scan parameters were 64 × 0.625 mm collimation, 0.9 mm slice thickness with 0.45 mm increment, 330 mm field-of-view, 0.392 pitch, 512 × 512 image matrix, high resolution and a rotation time of 0.75 s. The hard and sharp reconstruction filter D was chosen in order to enhance edges and to optimize the contrast between hard and soft materials in the CT imaging of metallic components. The iterative reconstruction algorithm contains a de-noising step which takes the noise in the spectral decomposition into account to de-noise the photoelectric and Compton images [17]. Without the use of the de-noising algorithm the noise heavily increases at low and high keV, which would result in a suboptimal results at very high keV regarding metal artefact reduction.

2.4. Quantitative analysis of the image quality

The effects of virtual monochromatic Spectral CT imaging, degree of metal artefacts and effectiveness in metal artefact reduction were quantified by analysing CT numbers, noise values, SNRs and CNRs within fixed regions of interest (ROIs) placed in and around the pellets (Fig. 2). The quantitative analysis was executed using the image-processing programs ImageJ (version 1.48 v) and Matlab® (version 2014b). A standardized measurement template mask was developed and used for each scan in order to enhance the reliability of the measurements. The coronal slice aligned at the middle of the pellets was stored at a Philips Intellispace Portal Workstation. A single coronal slice was loaded into ImageJ where a template was manually created with 9 left pellet ROIs (L0–L8) and 9 right pellet ROIs (R0–R8) (Fig. 2a). Matlab was used to perform the actual quantitative measurements. Pellet ROIs had a diameter of 14.7 pixels or 6.6 mm thus mitigating partial volume effects. The number of pixels of background ROIs was matched to the number of pixels of pellet ROIs. Fig. 2b illustrates a single pellet with its inner pellet ROI 1 and surrounding background ROI 2. CT numbers were calculated by measuring mean pixel intensities within local ROIs (Eq. (1)). Noise was measured by calculating the standard deviation of pixels in an ROI of a uniform section of the image (Eq. (2)).
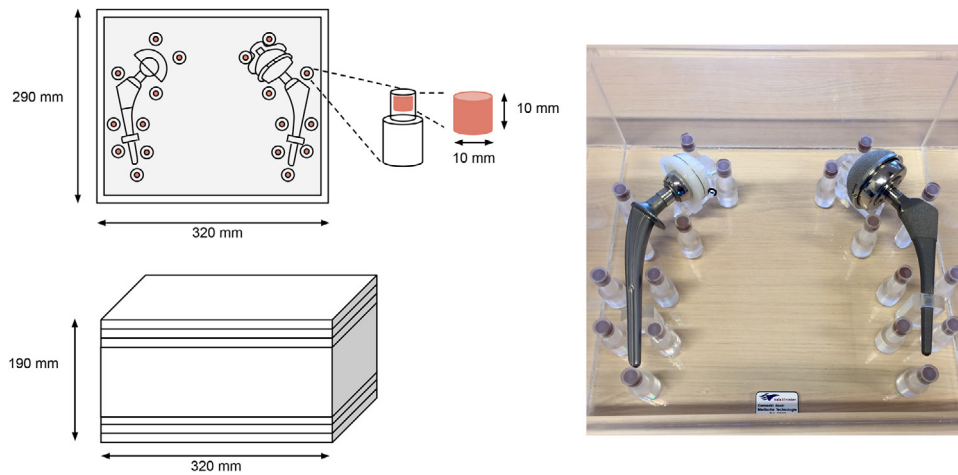
Fig. 1. The total hip arthroplasty phantom with dimensions. A water-filled phantom was used made of polymethyl methacrylate (PMMA) or Perspex containing different prosthesis surrounded by 18 hydroxyapatite/calcium carbonate pellets representing bone. Three PMMA shields with a thickness of 10 mm were placed on top and beneath the original phantom box to represent more clinical relevant phantom dimensions. The cylindrical pellets with a height and diameter of 10 mm were mounted on PMMA pillars.

Table 1
The in total 6 different phantom configurations using three different hip prostheses consisting of different metal alloys.

Prosthesis R	Setting	Prosthesis L	Prosthesis R	Setting	Prosthesis L
	Box 1			Box 4	
Cup: − Head: − Stem: −		Cup: − Head: − Stem: −	Cup: − Head: − Stem: −		Cup: CoCrMo[b] Head:CoCrMo[b] Stem: TiAlV[d]
	Box 2			Box 5	
Cup: UHMWPE[a] Head: CoCrMo[b] Stem: CoCrMo[b]		Cup: − Head: − Stem: −	Cup: UHMWPE[a] Head: ZTA[c] Stem: TiAlV[d]		Cup: CoCrMo[b] Head: CoCrMo[b] Stem: TiAlV[d]
	Box 3			Box 6	
Cup: UHMWPE[a] Head: ZTA[c] Stem: CoCrMo[b]		Cup: CoCrMo[b] Head: CoCrMo[b] Stem:TiAlV[d]	Cup: UHMWPE[a] Head: ZTA[c] Stem: TiAlV[d]		Cup: − Head: − Stem: −

[a] Ultra-High-Molecular-Weight-Poly-Ethylene.
[b] Cobalt-Chrome-Molybdenum.
[c] Zirconia-Toughened-Alumina.
[d] Titanium-Aluminium-Vanadium.

SNRs were calculated by dividing average CT numbers within pellet ROIs by noise values in the pellet ROIs (Eq. (3)). Contrast was defined as the absolute difference in CT number in HU between the pellet and its surrounding background. Local CNRs were calculated by subtracting the average CT number of the local background from the average CT number of the pellet and subsequently dividing this by the noise of the local background ROI (Eq. (4)). In Eqs. (1)–(4), 'p' and 'b' are referred as pellet and background respectively.

2.5. Quantifying metal artefact reduction

Virtual monochromatic images were generated and analysed from the range of 40–200 keV with steps of 10 keV. Mean monochromatic energies of 70 and 74 keV were found to produce similar CT numbers of the pellets comparable to 120-kVp and 140-kVp polychromatic results respectively. Quantitative measurements obtained from virtual monochromatic images at 70 and 74 keV therefore served as a reference for respectively 120-kVp and 140-kVp acquisitions.

Each of the 108 individual pellets of Box 1–6 were categorized in degree of metal artefact severity based on mean CT numbers of the pellet ROIs in virtual monochromatic images at 70 and 74 keV. Pellets with CT numbers greater than 250 HU were categorized as 'unaffected' or 'no artefacts' (A) since CT numbers smaller than 250 HU deviate more than a standard deviation compared to reference values. Pellets with CT numbers in between 250 and −600 HU
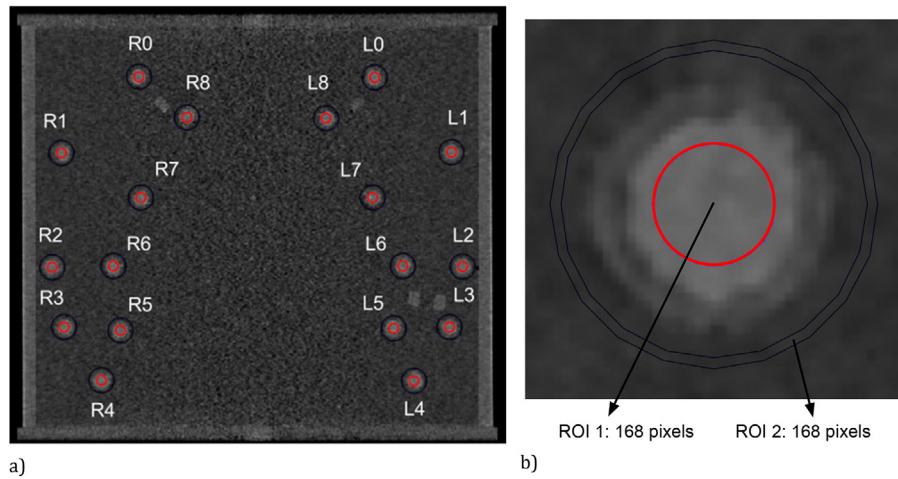
Fig. 2. A coronal 74 kiloelectron volt (keV) monochromatic image acquired at 140-kVp and a Computed Tomography dose index (CTDI) of 20.0 mGy reconstructed with iterative reconstruction. Fig. 2a illustrates the measurement template mask including the regions of interest (ROIs) of the 18 pellets, 9 left pellets (L0–L8) and 9 right pellets (R0–R8). Fig. 2b illustrates a single pellet with the inner pellet ROI 1 and outer background ROI 2. The number of pixels of the background ROI 2 was adapted to the inner pellet ROI 1.
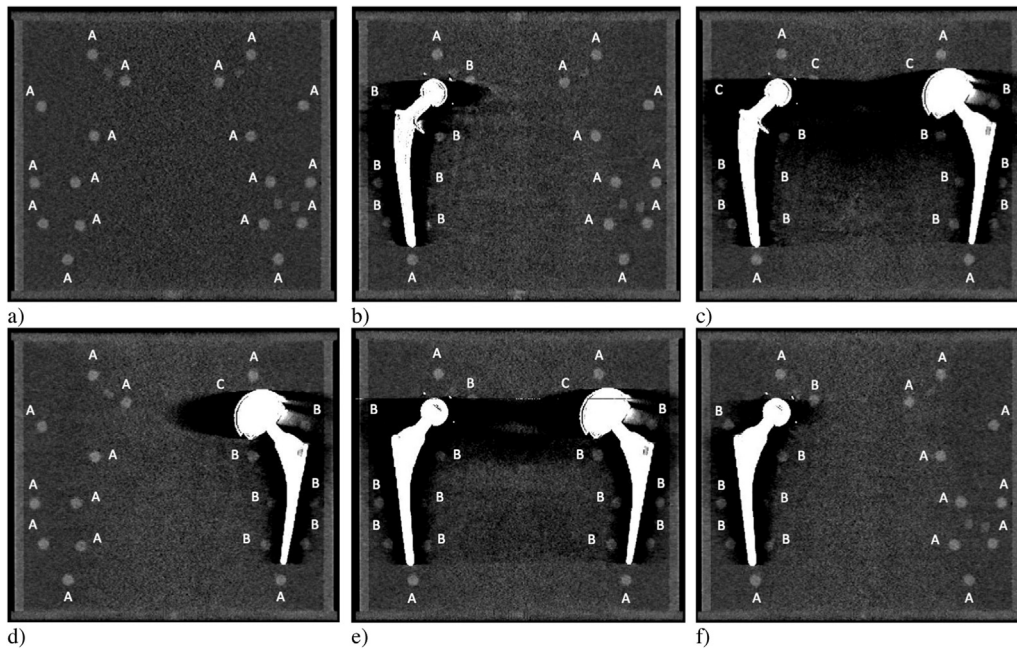

Fig. 3. Categorization of all pellets in 74 keV monochromatic images acquired at 140-kVp and a CTDI of 20.0 mGy for Box 1–6 shown in Fig. 3a–f respectively. The 18 pellets of each box were categorized by measuring pixel intensities and named unaffected or reference (A), mild/moderate artefacts (B) and severe artefacts (C).

were categorized as 'mild/moderate artefacts' (B). A threshold of −600 HU was chosen based on an observed difference in HU trend for pellets with CT numbers lower than −600 HU. Pellets with CT numbers smaller than −600 HU were categorized as 'severe' artefacts' (C). Fig. 3 illustrates the categorization in degree of metal artefacts for all boxes in 74 keV images acquired at 140-kVp. Fig. 4 illustrates the categorization of all pellets for 120-kVp and 140-kVp results.

Metal artefact reduction was calculated by analysing differences in CT numbers, noise values, SNRs and CNRs of affected pellets compared to unaffected pellets. These differences at high keVs were compared to differences at reference keVs in order to quantify metal artefact reduction (Eq. (5)). In Eq. (5), 'V$_u$' and 'V$_a$' are referred

as the 'Values' of mean CT number, noise, SNR and CNR of unaffected and affected pellets respectively.

$$CT\ number = HU_{p,b} \tag{1}$$

$$Noise = \sigma_{p,b} \tag{2}$$

$$SNR = \frac{HU_p}{\sigma_p} \tag{3}$$

$$CNR = \frac{HU_p - HU_b}{\sigma_b} \tag{4}$$

$$Metal\ artefact\ reduction\ (\%) = \left(1 - \left(\frac{|V_u - V_a|_{high\ keV}}{|V_u - V_a|_{reference\ keV}}\right)\right)$$
$$\times 100\% \tag{5}$$
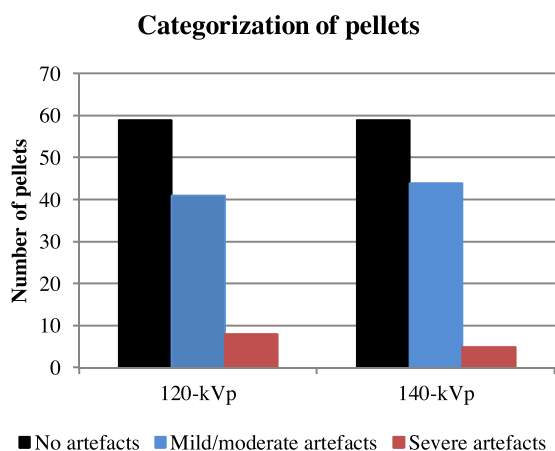
Categorization of pellets

Fig. 4. Categorization (no, mild/moderate and severe artefacts) of all 108 pellets for 120-kVp and 140-kVp acquisitions. Categorized pellets were summed for all 6 boxes, 108 pellets in total for each kVp. For 120-kVp results or 70 keV monochromatic images, 59, 41, and 8 pellets out of the 108 pellets were categorized in respectively no, mild/moderate and severe artefacts. For 140-kVp results or 74 keV monochromatic images, 59, 44 and 5 out of the 108 pellets were categorized in respectively no, mild/moderate and severe artefacts.

2.6. Statistical analysis

Results are presented in figures and graphs. Statistical analysis was performed by means of a Wilcoxon signed-ranks test. A two-sided alpha of 5% was used as significance level.

3. Results

Quantitative measurements of CT numbers, noise values, SNRs and CNRs of the hydroxyapatite/calcium carbonate pellets, without the insertion a prosthesis, varied over the spectrum from 40 to 200 keV. Reference CT numbers of the pellets measured without the insertion of a prosthesis in 70 keV monochromatic images, corresponding to 120-kVp acquisitions, were 289 ± 11 HU. In 74 keV monochromatic images, corresponding to 140-kVp acquisitions, reference CT numbers were 266 ± 11 HU. CT numbers of the pellets were high at 40 keV and decreased at higher keVs for both 120-kVp and 140-kVp results. CT numbers of water remained unaffected over the entire keV spectrum. Noise was higher for 120-kVp results compared to 140-kVp results at similar dose levels and remained constant. As with CT numbers, SNRs and CNRs decreased at higher keV levels. At 40 keV, SNRs and CNRs were more than 2 times higher compared to reference values at 70 and 74 keV results mainly due to a high contrast between the pellets and local backgrounds.

3.1. Metal artefact reduction

For 120-kVp results, artefacts regarding CT numbers, noise values, SNRs and CNRs for mild and moderate artefacts were reduced with 68%, 62%, 65% and 66% respectively at 200 keV ($p < 0.001$). Artefacts regarding CT numbers, noise values, SNRs and CNRs in severe artefacts were reduced with 11%, 4%, 13% and 41% respectively at 200 keV ($p < 0.001$). Fig. 5 shows CT numbers, noise values, SNRs and CNRs from 74 keV up to 200 keV of pellets categorized as 'no artefacts', 'mild/moderate artefacts' and 'severe artefacts' acquired at 140-kVp. For 140-kVp results, artefacts regarding CT numbers, noise values, SNRs and CNRs for mild and moderate artefacts were reduced with 75%, 63%, 74% and 71% respectively at 200 keV ($p < 0.001$) (Fig. 5). Artefacts in CT numbers, noise values, SNRs and CNRs in severe artefacts were reduced with 6%, 6%, 4% and 36% respectively at 200 keV ($p < 0.001$) (Fig. 5). Fig. 6(a–f) illustrates 130 keV images of the 6 Boxes acquired at 140-kVp. Severe metal

artefacts seemed to be reduced since differences between unaffected and severe pellets were reduced at higher keVs. However, this reduction was clinically irrelevant due to the overall decrease in contrast, thereby strongly decreasing CT numbers, SNRs and CNRs of unaffected pellets also. Absolute CT numbers, SNRs and CNRs of severe pellets were lowered and further decrease at high keVs.

3.2. Optimal keV selection

Although the 200 keV monochromatic images resulted in the smallest differences in CT numbers, noise and CNRs between mild/moderate and unaffected pellets, the image contrast for all pellets (affected and unaffected) was strongly reduced at these high keVs. The overall optimal keV selection was based on a quantitative analysis on CT numbers, noise values, SNRs and CNRs. CNR outcomes were decisive since it simultaneously includes noise and contrast values. CNRs, illustrated in Fig. 5, of all pellets categorized as mild/moderate artefacts in 140-kVp results showed an optimum at 130 keV with a CNR of 3.0 ± 1.2 and showed a slight decrease at higher keVs. Overall contrast between unaffected pellets and local backgrounds at 130 keV was reduced with 36% and was reduced with 45% at 200 keV. CNRs were 17% higher at 130 keV and 14% higher at 200 keV, compared to 74 keV results. At 130 keV in 140-kVp acquisitions, deviations in CT numbers, noise values, SNRs and CNRs of mild/moderate artefacts compared to unaffected pellets were decreased with 64%, 57%, 62% and 63% respectively (Figs. 5 and 6) ($p < 0.001$).

Fig. 7a–d shows respectively CT numbers, noise values, SNRs and CNRs of mild/moderate affected pellets for Box 2–6 and reference values of unaffected pellets. Results are clearly best for the Titanium-Aluminium-Vanadium prosthesis with an Alumina-Ceramic head and UHMWPE cup referred as Box 6 with highest CT number accuracy, SNRs and CNRs and lowest noise values. Fig. 8 illustrates Box 6 at 140-kVp at monochromatic energies of 40, 74, 110, 130 and 200 keV. Results are clearly poorest for the Cobalt-Chrome-Molybdenum prosthesis with a Cobalt-Chrome-Molybdenum head and UHMWPE cup referred as Box 2 with lowest CT number accuracy, SNRs and CNRs and highest noise values. Optimal CNRs for Box 2–6 were respectively 74 keV, 130 keV, 140 keV, 150 keV and 110 keV (Fig. 7d).

4. Discussion

We found that virtual monochromatic dual-layer detector Spectral CT imaging reduces mild and moderate metal artefacts significantly as the keV increases in the CT imaging of a unilateral and bilateral hip prostheses phantom representing a patient with a body mass index of 25 ($p < 0.001$). Streak-artefacts were reduced by reducing beam-hardening effects. The use of 140-kVp acquisitions and an average virtual monochromatic energy level of 130 keV (ranging from 74 to 150 keV for different prosthetic configurations) resulted in optimal CNRs in the CT imaging of metal hip prostheses with metal artefact reduction capabilities and simultaneously limited loss of overall image contrast. In 130 keV results, only mild/moderate metal artefacts were significantly reduced where deviations in CT numbers, noise, SNRs and CNRs compared to unaffected pellets were decreased with respectively 64%, 57%, 62% and 63% ($p < 0.001$) (Fig. 5). High keV monochromatic images did not show a significant reduction in case of severe metal artefacts. CT numbers of the pellets and overall image contrast were strongly reduced at high keVs due to a reduced photon attenuation by the pellets at high photon energies. Signal-to-noise-ratios and contrast-to-noise-ratios mainly decreased due to a loss in overall image contrast since the noise component remained constant. The constant noise level of unaffected pellets over the entire keV spec-
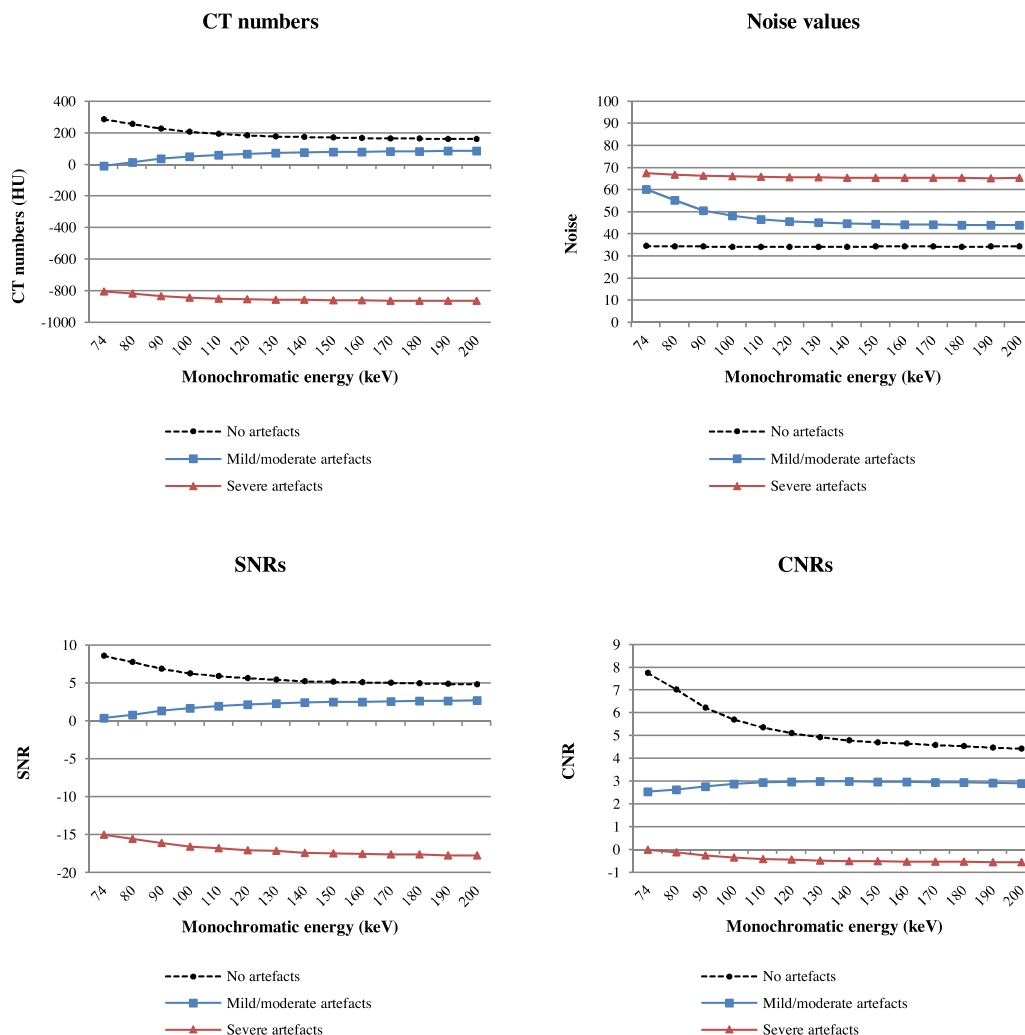
CT numbers

Noise values

SNRs

CNRs

Fig. 5. Average CT numbers (a), noise values (b), signal-to-noise-ratios (SNRs) (c) and contrast-to-noise-ratios (CNRs) (d) of all pellets categorized as 'no artefacts', 'mild/moderate artefacts' and 'severe artefacts'. Virtual monochromatic results from 74 keV up to 200 keV acquired at 140-kVp are shown. (a) CT numbers of unaffected pellets decreased at high keVs. Also CT numbers of pellets categorized as severe artefacts decreased at high keVs. CT numbers of pellets in mild/moderate artefacts increased with increasing keVs. (b) Noise values of unaffected pellets remained constant from 74 up to 200 keV. Noise values of pellets categorized as severe artefacts were high and remained constant. Noise values of pellets in mild/moderate artefacts decreased with increasing keVs. (c) SNRs of unaffected pellets decreased at high keVs. Also SNRs of pellets categorized as severe artefacts decreased at high keVs. SNRs of pellets in mild/moderate artefacts increased with increasing keVs. (d) CNRs of unaffected pellets decreased at high keVs. Also CNRs of pellets categorized as severe artefacts decreased at high keVs. CNRs of pellets in mild/moderate artefacts increased with increasing keVs with a peak CNR of 3.0 at 130 keV.

trum confirms the effectiveness of the de-noising algorithm. To the best of our knowledge this is the first study quantifying metal arte-fact reduction by use of dual-layer detector Spectral CT on outcome values such as CT numbers, noise values, SNRs and CNRs.

We categorized three categories of metal artefacts: unaffected or no artefacts, mild/moderate artefacts and severe artefacts, based on cut-off values of CT numbers of the pellets in 70 and 74 keV virtual monochromatic images for respectively 120-kVp and 140-kVp polychromatic acquisitions. Virtual monochromatic imaging at high keVs only showed a positive effect for mild/moderate arte-facts by increasing CT numbers, SNRs and CNRs and decreasing noise values (Fig. 5). In severe artefacts, CT number accuracy, SNRs and CNRs were degraded even further where noise values were high and remained unchanged at higher keVs (Fig. 5). A greater thickness in metal, especially around the head of the metal-on-metal-prosthesis used in Box 4, resulted in a higher attenuation of photons, which subsequently resulted in more severe artefacts. The Cobalt-Chrome-Molybdenum alloy used in the stem of the prosthe-

sis in Box 2 and 3 and the head of the prosthesis used in Box 3 and 4 resulted in more severe artefacts compared to the Aluminium-Titanium-Vanadium alloy parts. This difference in metal artefact severity can be explained by a greater atomic weight in case of the Cobalt-Chrome-Molybdenum alloy with a higher attenuation of photons, which is supported by a similar study by Huang et al. [10]. The effectiveness of high keV virtual monochromatic imaging in reducing metal artefacts strongly depends on the thickness of the prostheses, the metallic alloy, the use of bilateral or unilateral prostheses and the distance and location relative to the prostheses.

Metal artefacts were more pronounced in 120-kVp acquisi-tions compared to 140-kVp acquisitions with greater CT number inaccuracies, higher noise values and lower SNRs and CNRs of mild/moderate and severely affected pellets. Fewer pellets were categorized as severe in 140-kVp acquisitions. In areas affected by metal artefacts, virtual monochromatic imaging at high keVs did not only improve CT numbers of the pellets, also the CT numbers of the local backgrounds were increased. Dark streaks were mitigated
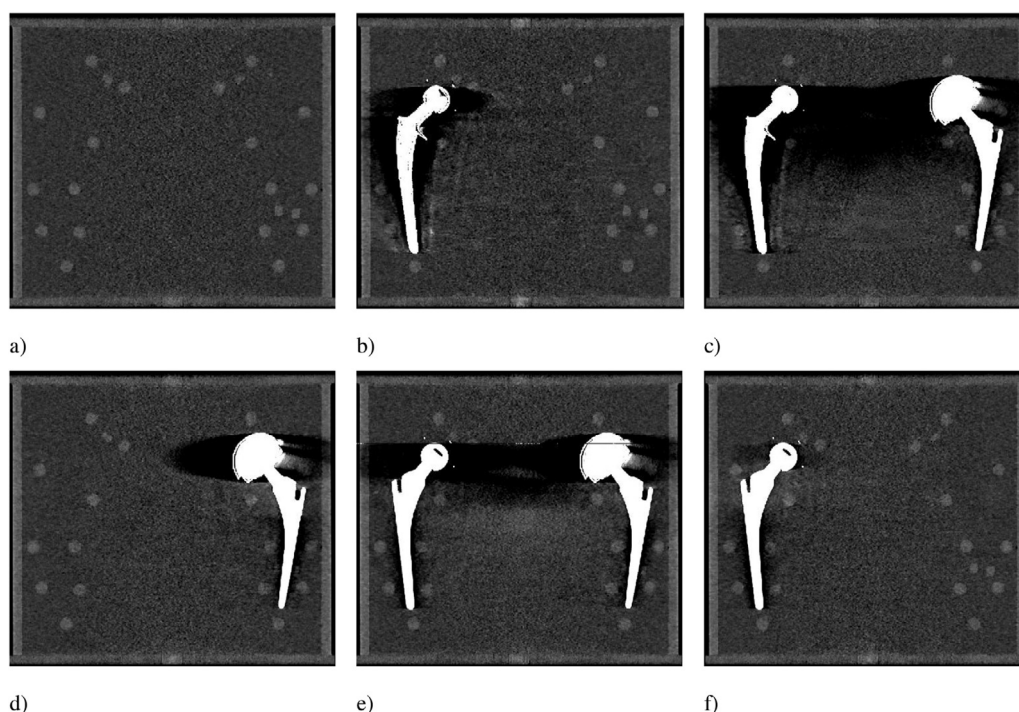
Fig. 6. Virtual monochromatic images at 130 keV of Box 1–6 shown in Fig. 6a–f respectively. Scans were acquired at 140-kVp and a CTDI of 20.0 mGy. Metal artefacts were reduced where the effectiveness in metal artefact reduction strongly depended on the kind of alloy, size and use of unilateral and bilateral metal hip prostheses. Overall images contrast was reduced compared to 74 keV monochromatic images shown in Fig. 3.

in the pellets and background. Virtual monochromatic imaging at the highest keV of 200 keV strongly reduced overall image contrast images and introduced a white haze in the middle of the prosthesis shown in Fig. 8. Mild/moderate metal artefacts were reduced up to 200 keV where greatest improvements in CT numbers, SNRs and CNRs and greatest noise reduction was observed in monochromatic images from 70/74 keV up to approximately 130 keV. From 140 keV up to 200 keV improvements in CT numbers, SNRs and CNRs and the further decrease of noise values were limited. In order to determine the detectability of a circular object, such as a pellet, from its surrounding environment the 'Rose criterion' can be applied. The Rose criterion states that in order to be detectable, the CNR of a circular object must exceed 3.0 [22,23]. Optimal keVs, based on CNRs, showed some variation between unilateral and bilateral prostheses and between the Aluminium-Titanium-Vanadium and Cobalt-Chrome-Molybdenum alloys as illustrated before (Fig. 7). In order to draw generic conclusions, an overall optimal keV was obtained by averaging the quantitative results of all investigated prosthetic configurations. CNRs of mild/moderate artefacts showed an optimum at 130 keV in 140-kVp acquisitions where CNRs of 3.0 ± 1.2 were reached. Overall image contrast further decreased from 140 up to 200 keV.

We found that by increasing the monochromatic energy metal artefacts in mild/moderate artefacts were reduced. Our results showed that, like other similar studies, virtual monochromatic imaging at high keVs subsequently reduced overall image contrast [1,9,11]. Our results are supported by results of Bamberg et al., Lewis et al., Wang et al., Andersson et al., Huang et al., Kuchenbecker et al. and Filograna et al., all investigate metal artefact reduction in metal hip prostheses using virtual monochromatic imaging [6,9–11,15,16,24]. However none of these studies focussed on virtual monochromatic imaging based on the dual-layer detector approach and most of these studies only focussed on HU measure-

ments only in case of quantitative analysis. Dual-layer detector CT imaging enables a spectral separation in the projection space without the need of spatial or temporal interpolations. It furthermore has the advantage that the spectral analysis can be applied retrospectively since spectral data is captured during each scan. However, the spectral separation cannot be adjusted and separation will be limited which results in more noise [25].

In a clinical setting, radiological evaluation of 130 keV monochromatic images in small unilateral hip implants consisting of lighter metals such as titanium, aluminium or vanadium will show reduced metal artefacts compared to 70 or 74 keV reference images. In case of large hip implants, bilateral hip implants and hip implants consisting of heavier metals such as cobalt, chrome or molybdenum metal artefact reduction is limited. In these cases, the use of higher keVs might result in some additional metal artefact reduction compared to 130 keV images. Metal artefacts caused by large metallic implants were reduced, but were still present since metal artefacts produced by photon-starvation and scatter still remained in the resultant images, also in high keV images. Therefore it is expected that metal artefact reduction capabilities of Spectral CT will be more effective in small metallic implants, such as pedicles and screws producing less severe artefacts. In previous phantom studies we have shown that the use of an orthopaedic metal artefact reduction algorithm significantly reduces metal artefacts by improving CT number accuracy, SNRs and CNRs while decreasing noise values in the conventional polychromatic multislice CT imaging of a large metal-on-metal hip prosthesis [19,26]. These results were supported by similar studies focussing on metal artefact reduction algorithms [6,10,11,14,27–30]. Since metal artefacts caused by photon-starvation and scatter are still present in high keV virtual monochromatic images, the combined use of additional software based metal artefact reduction approaches will likely improve the effectiveness in metal artefact reduction in
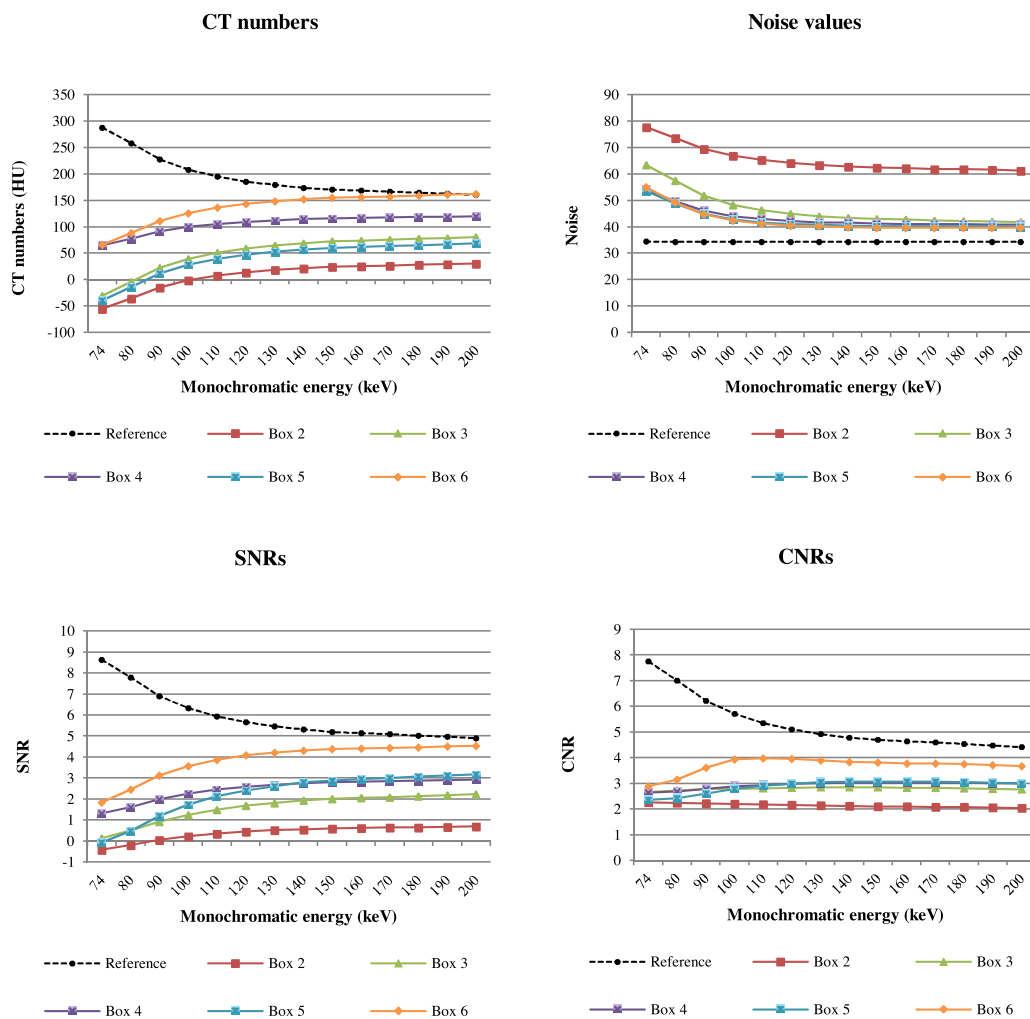
CT numbers

Noise values

SNRs

CNRs

Fig. 7. Average CT numbers (a), noise values (b), SNRs (c) and CNRs (d) of all unaffected pellets (reference) and pellets categorized as 'mild/moderate artefacts' for Box 2–6. Virtual monochromatic results from 74 keV up to 200 keV acquired at 140-kVp are shown. (a) CT numbers of pellets in mild/moderate artefacts increased with increasing keVs for all boxes. (b) Noise values of pellets in mild/moderate artefacts decreased with increasing keVs for all boxes. (c) ScNRs of pellets in mild/moderate artefacts increased with increasing keVs for all boxes. (d) CNRs of pellets in mild/moderate artefacts increased with increasing keVs except for Box 2, with a peak CNRs at 74 keV, 130 keV, 140 keV, 150 keV and 110 keV for respectively Box 2–6.

dual-layer detector Spectral CT systems, especially in large metal hip prostheses. A clinical study can give more insights to further validate and optimize dual-layer detector Spectral CT imaging in patients with total hip prostheses and other metal hardware.

Our study has limitations. We have only performed quantitative analysis by measuring CT numbers, noise values, SNRs and CNRs using a standardized measurement template. The standard deviation of pixels within an ROI is a combination of noise and artefact. By addressing noise as the standard deviation of pixels within a ROI only, we were not able to determine whether virtual monochromatic imaging at high keVs actually reduced noise in by metal affected regions or if it only reduced the artefact resulting in a reduced standard deviation of pixels within that region. Additional subjective image quality scoring can give more insights in the clinical usefulness and additional value of virtual monochromatic Spectral CT imaging in reducing metal artefacts in patients. The hydroxyapatite/calcium carbonate pellets with a high density resulted in high contrast values between the pellets and its background. Adding pellets with different densities or adding soft tissue can give more insights in the possible additional clinical value in patients. Performing an identical quantitative phantom study on

dual-source, kVp-switching, dual-spin and beam pre-filtration systems can give more insights in intrinsic strengths and weaknesses in metal artefact reduction for different Dual-Energy approaches. Furthermore, we feel the necessity to use additional software based metal artefact reduction approaches. However, combining these approaches with dual-layer Spectral CT imaging is currently not yet available.

Virtual monochromatic dual-layer Spectral CT imaging results in a significant reduction of streak artefacts produced by beam-hardening in mild and moderate artefacts by improving CT number accuracy, SNRs and CNRs, while decreasing noise values in a total hip arthroplasty phantom. An optimal monochromatic energy of 130 keV was found ranging from 74 keV–150 keV for different unilateral and bilateral hip prostheses consisting of different metal alloys.

Disclosures of conflicts of interest

R.H.H.W. No relevant conflicts of interest to disclose.
M.F.B. No relevant conflicts of interest to disclose.
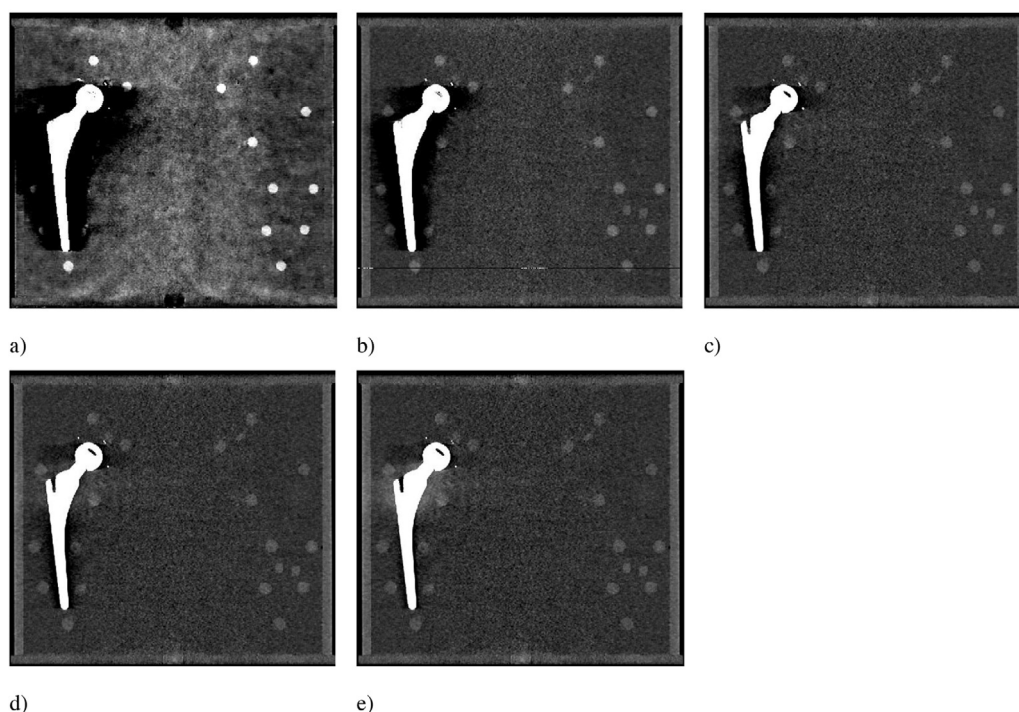J.A.C.O. No relevant conflicts of interest to disclose.

Fig. 8. Virtual monochromatic images at 40, 74, 110, 130 and 200 keV of Box 6 shown in Fig. 8a–e respectively. Scans were acquired at 140-kVp and a CTDI of 20.0 mGy.

References

[1] F.E. Boas, D. Fleischmann, CT artifacts: causes and reduction techniques, Imaging Med. 4 (2012) 229–240.
[2] R. Molteni, From CT numbers to hounsfield units in cone beam volumetric imaging: the effect of artifacts, in: 62th AAOMR, Chicago, 2011, 2011.
[3] M. Bruesewitz, L. Yu, S. Leng, J. Kofler, T. Vrieze, J. Fletcher, et al., Virtual Monochromatic Imaging in Dual-Energy CT: Radiation Dose, Image Quality, and Clinical Applications, Dep. Radiol. Mayo Clin. Coll. Med. Mayo Clin., Rochester, MN, Mayo Found, 2012.
[4] M.M. Goodsitt, E.G. Christodoulou, S.C. Larson, Accuracies of the synthesized monochromatic CT numbers and effective atomic numbers obtained with a rapid kVp switching dual energy CT scanner, Med. Phys. 38 (2011) 2222–2232.
[5] R. Raupach, C.R. Becker, T.R. Johnson, B. Krauss, T. Flohr, B. Schmidt, Metal artifact reduction for dual source dual energy computed tomography, in: H. Hricak (Ed.), 96th Scientific Assembly and Meeting of the Radiological Society of North America, Radiol. Soc. North Am., Oak Brook, 2010.
[6] F. Bamberg, A. Dierks, K. Nikolaou, M.F. Reiser, C.R. Becker, T.R. Johnson, Metal artifact reduction by dual energy computed tomography using monoenergetic extrapolation, Eur. Radiol. 21 (2011) 1424–1429.
[7] E. Pessis, R. Campagna, J. Sverzut, F. Bach, M. Rodallec, H. Guerini, et al., Virtual monochromatic spectral imaging with fast kilovoltage switching: reduction of metal artifacts at CT, Radiographics 33 (2013) 573–583.
[8] T.M. Coupal, P.I. Mallinson, P. McLaughlin, S. Nicolaou, P.L. Munk, H. Ouellette, Peering through the glare: using dual-energy CT to overcome the problem of metal artefacts in bone radiology, Skelet. Radiol. 43 (2014) 567–575.
[9] S. Kuchenbecker, S. Faby, S. Sawall, M. Lell, M. Kachelrieß, Dual energy CT: how well can pseudo-monochromatic imaging reduce metal artifacts? Med. Phys. 42 (2015) 1023–1036.
[10] J. Huang, J. Kerns, J. Nute, X. Liu, P. Balter, F. Stingo, et al., An evaluation of three commercially available metal artifact reduction methods for CT imaging, Phys. Med. Biol. 60 (2015) 1047–1067.
[11] M. Lewis, K. Reid, A. Toms, Reducing the effects of metal artefact using high keV monoenergetic reconstruction of dual energy CT (DECT) in hip replacements, Skelet. Radiol. 42 (2013) 275–282.
[12] R. Guggenberger, S. Winklhofer, G. Osterhoff, G.a. Wanner, M. Fortunati, G. Andreisek, et al., Metallic artefact reduction with monoenergetic dual-energy CT: systematic ex vivo evaluation of posterior spinal fusion implants from various vendors and different spine levels, Eur. Radiol. 22 (2012) 2357–2364.
[13] Y.H. Lee, K.K. Park, H.-T. Song, S. Kim, J.-S. Suh, Metal artefact reduction in gemstone spectral imaging dual-energy CT with and without metal artefact reduction software, Eur. Radiol. 22 (2012) 1331–1340.
[14] S.C. Han, Y.E. Chung, Y.H. Lee, K.K. Park, M.J. Kim, K.W. Kim, Metal artifact reduction software used with abdominopelvic dual-energy CT of patients with metal hip prostheses: assessment of image quality and clinical feasibility, AJR Am. J. Roentgenol. 203 (2014) 788–795.
[15] F. Wang, H. Xue, X. Yang, W. Han, B. Qi, Y. Fan, et al., Reduction of metal artifacts from alloy hip prostheses in computer tomography, J. Comput. Assist. Tomogr. 38 (2014) 823–833.
[16] L. Filograna, N. Magarelli, A. Leone, R. Guggenberger, S. Winklhofer, M.J. Thali, et al., Value of monoenergetic dual-energy CT (DECT) for artefact reduction from metallic orthopedic implants in post-mortem studies, Skelet. Radiol. 44 (2015) 1287–1294.
[17] A. Vlassenbroek, Spectral Detector CT (SDCT), (2013) 1–50.
[18] J. Menke, Comparison of different body size parameters for individual dose adaptation in body CT of adults, Radiology 236 (2005) 10–14.
[19] M.F. Boomsma, N. Warringa, B.J. Kollen, J. van Dalen, D. Mueller, A. Vlassenbroek, et al., Quantitative analysis of orthopedic metal artifact reduction in 64-slice computed tomography scans in large head metal-on-metal total hip replacements, a phantom study, Springerplus 2 (April (5)) (2016) 405.
[20] T. Gruen, G. McNeice, H. Amstutz, Modes of failure of cemented stem-type femoral components: a radiographic analysis of loosening, Clin. Orthop. Relat. Res. 141 (1979) 17–27.
[21] J. DeLee, J. Charnley, Radiological demarcation of cemented sockets in total hip replacement, Clin. Orthop. Relat. Res. 121 (1976) 20–32.
[22] S. Cherry, M. Phelps, J. Sorenson, Phys. Nucl. Med. (Fourth edition) (2012) 233–251.
[23] A.E. Burgess, The rose model, revisited, Opt. Soc. Am. 16 (1999) 633–646.
[24] K.M. Andersson, P. Nowik, J. Persliden, P. Thunberg, E. Norrman, Metal artefact reduction in CT imaging of hip prostheses—an evaluation of commercial techniques provided by four vendors, Br. J. Radiol. 88 (2015).
[25] M.M. Lell, J.E. Wildberger, H. Alkadhi, J. Damilakis, M. Kachelriess, Evolution in computed tomography: the battle for speed and dose, Invest. Radiol. 50 (2015) 629–644.
[26] R.H.H. Wellenberg, M.F. Boomsma, J.A.C. van Osch, J. Milles, A. Vlassenbroek, M.A. Edens, et al., Metal artefact reduction in CT-imaging of a hip prothesis using iterative model-based reconstruction and orthopaedic metal artefact reduction: a quantitative analysis, J. Comput. Assist. Tomogr. 40 (6) (2016) 971–978.
[27] F. Morsbach, S. Bickelhaupt, G.A. Wanner, Reduction of metal artifacts from hip prostheses on CT images of the pelvis: value of iterative reconstructions, Radiology 268 (2013) 237–244.
[28] P.T. Liu, W.P. Pavlicek, M.B. Peter, M.J. Spangehl, C.C. Roberts, R.G. Paden, Metal artifact reduction image reconstruction algorithm for CT of implanted metal orthopedic devices: a work in progress, Skele. Radiol. 38 (2009) 797–802.

[29] P. Gondim Teixeira, J. Meyer, C. Baumann, A. Raymond, F. Sirveaux, H. Coudane, et al., Total hip prosthesis CT with single-energy projection-based metallic artifact reduction: impact on the visualization of specific periprosthetic soft tissue structures, Skelet. Radiol. 43 (2014) 1237–1246.

[30] M. Kidoh, T. Nakaura, S. Nakamura, S. Tokuyasu, H. Osakabe, K. Harada, et al., Reduction of dental metallic artefacts in CT: value of a newly developed algorithm for metal artefact reduction (O-MAR), Clin. Radiol. 69 (2014) e11–e16.